Programmable Cellular Retention of Nanoparticles by Replacing the Synergistic Anion of Transferrin

Li-Chen Wu,[†,*] Li-Wei Chu,[‡] Leu-Wei Lo,[§] Yen-Chen Liao,[†] Yu-Chao Wang,[‡] and Chung-Shi Yang[‡,⊥,*]

[†]Biochemistry Laboratory, Department of Applied Chemistry, National Chi Nan University, Puli, Nantou 54561, Taiwan, [‡]Center for Nanomedicine Research, National Health Research Institutes, Zhunan, Miaoli 35053, Taiwan, [§]Division of Medical Engineering Research, National Health Research Institutes, Zhunan, Miaoli 35053, Taiwan, and [⊥]Department of Applied Chemistry, National Chi Nan University, Puli, Nantou 54561, Taiwan

ABSTRACT The ability to program the intracellular retention of nanoparticles (NPs) would increase their applicability for imaging and therapeutic applications. To date, there has been no efficient method developed to control the fate of NPs once they enter cells. Existing approaches to manipulate the intracellular retention of NPs are mostly "passive" and particle size-dependent. Different sized particles hold distinct cellular responses. The adverse effect of particle size may limit the utility of nanodelivery systems. Therefore, the development of tunable/"active" NP intracellular retention systems with fixed particle sizes remains a considerable challenge. By replacing the synergistic anions of transferrin (Tf) immobilized on quantum dots (Tf-QDs, *ca.* 25 nm), we have examined the feasibility of this concept. Substitution of synergistic anions of Tf from carbonate (holo-Tf) to oxalate (oxa-Tf) significantly increased the intracellular accumulation of the oxa-Tf-QDs as a result of (i) a delay in cellular removal triggered by oxalate (oxa-Tf)-induced endosomal Tf iron-release retardation and (ii) enhanced recycling of Tf-QD/TfR (Tf receptor) complexes from early endosomes to the plasma membrane. This accumulation extended the intracellular NP retention interval. The half-maximum fluorescence intensity of the oxa-Tf-QDs *in vivo* was 4 times higher than that of the holo-Tf-QDs. Programming of the intracellular NP retention time was accomplished through manipulation of the ratio of holo- and oxa-Tfs on the surfaces of the QDs. Using this simple and efficient approach, it was possible to readily achieve a desirable intracellular retention interval for the NPs.

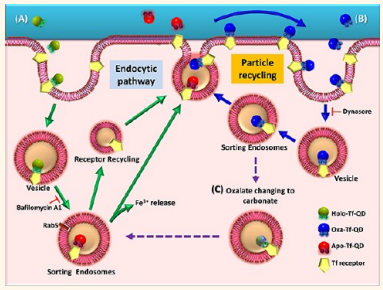

KEYWORDS: programmable particle intracellular retention · oxalate · transferrin · synergistic anion · iron-release retardation

The biomedical efficacy of modern nanoparticle (NP)-derived therapeutics relies on the successful delivery of the NPs to target tissues and cells.[1,2] The intracellular retention of NPs determines their release efficiency, as well as the intracellular accumulation of imaging and therapeutic agents.[2−7] Although active delivery systems increase intracellular drug accumulation, the exposed ligands may also lead to an overall decrease in tumor cellular uptake, due to accelerated NP opsonization and blood clearance.[8,9] The remaining functional NPs would undergo an unsatisfactory degree of accumulation, generally less than 10% injected dose/gram of tumor tissue.[10] Therefore, considerable efforts have been devoted to designing nanoformulations to improve the targeting efficiency and drug accumulation of NPs through decreased blood clearance and withholding by the reticuloendothelial system.[11] An alternative approach to enhancing the accumulation of NPs would be to manipulate the intracellular NP retention intervals, a fundamental, yet much less investigated, area.

Unlike active and passive NP delivery systems, which are usually developed through manipulation of the nanomaterials' physicochemical properties (*e.g.*, size, shape, surface), the existing approaches toward regulating the intracellular retention of nanomaterials are mostly particle size-dependent.[12] These particles with defined sizes "passively" control their intracellular retention periods (*i.e.*, they are regulated by default cell behavior). Particles that are 50 nm in size demonstrate superior cell uptake rate than other sized particles such as 14 and 74 nm.[12,13] However these NPs (50 nm) tend to be restricted in cells and cause nanocytotoxicity.[13] On the other hand, smaller (<50 nm) NPs result in less apoptosis but are apt to pass out of cells.[14] Additionally, NPs having hydrodynamic diameters of 20 nm demonstrate more rapid

* Address correspondence to lw25@ncnu.edu.tw, cyang@nhri.org.tw.

Received for review September 19, 2012 and accepted November 29, 2012.

Published online November 29, 2012
10.1021/nn3043397

tumor permeation than the restricted permeation of other sized particles (40, 60, 80, 100 nm).[15] Thus, there is an urgent need to develop a strategy to combine the advantages of different-sized NPs to improve imaging and therapeutic efficacy; as a result, smaller NPs might possibly experience an extended intracellular retention period and improved cellular accumulation. In addition, prolonged intracellular retention can markedly enhance the efficacy of biocompatible materials, such as mesoporous silica nanoparticles.[16]

At present, there is no efficient approach to "actively" regulate the intracellular NP retention periods to attain a desirable NP accumulation. A potential means of actively controlling the intracellular retention of nanomaterials could be achieved through manipulation of ligand−receptor interactions, especially those of intracellular recycling ligand−receptor complexes, against cell behavior. Receptors, such as transferrin receptor (TfR), can be recycled from the early endosomes to the cell surfaces in preparation for the next binding event. Transferrin, a widely used biorecognition molecule for enhancing the efficacy of nanodelivery,[17−20] binds to TfR on the cell surface with the presence of two ferric (Fe^{3+}) ions. The resulting Tf/TfR complex is subsequently internalized to early endosomes *via* clathrin-mediated endocytosis. After the release of iron through acidification of the endosomes, the apo-Tf/TfR complex can return to the cell surface, where the components dissociate upon exposure to the neutral pH;[21,22] receptors later participate in another cycle of iron uptake. Enhanced transferrin (Tf)−TfR binding can facilitate Tf cycling in cells, resulting in extended Tf cellular retention.[23] Consequently, Tf-modified NPs are capable of altering their intracellular retention through a similar mechanism. Meanwhile, the low pH of early endosomes (pH 6.0) can assist pharmaceutical carriers in releasing their cargoes through cleavage of a stimuli-sensitive bond, such as a pH-sensitive hydrazone (pH 5.0−6.0).[24]

Previous studies have revealed that the Fe^{3+} ion in the metal binding site of Tf is anchored by six coordination sites; four are from conserved amino acid residues, and the other two are from bound synergistic anions, usually carbonate *in vivo*.[22] Substitution of the synergistic anions with oxalate can strengthen the binding of the Fe^{3+} ions to Tf because of the oxalate anion's low pK_a and symmetric bidentate mode of binding.[22,25−27] Replacing Tf carbonate with oxalate enhances the stability of the Tf/TfR complexes. Using this approach, the intracellular retention time of Tf-coated nanostructures might possibly be controlled. Programming of the intracellular retention time of NPs would then become feasible through adjustment of the carbonate-/oxalate-Tf ratio on the surfaces of the nanostructures.

In this study, we attempted to develop a nanoplatform for programmable intracellular NP retention. By manipulating the synergistic anions of Tf, we found that oxalate-Tf-modified quantum dots (oxa-Tf-QDs) experienced extended intracellular retention both *in vitro* and *in vivo*. This extension was due to the delay in NP cellular removal triggered by (i) oxalate (oxa-Tf)-induced retardation of endosomal Tf iron release and (ii) recycling of Tf/TfR complexes from early endosomes to the plasma membrane. We could control the programming of the intracellular NP retention time by manipulating the ratio of oxalate- and carbonate-Tf species on the surfaces of QDs. To the best of our knowledge, this paper reports the first demonstration of the regulation of intracellular NP retention through manipulation of ligand−receptor interactions, rather than through variations of particle sizes, shapes, and charges. The information obtained herein might provide guidance to advance the development of nanobiomedicinal carriers and devices. In addition, this method should be a simple one for programming nanostructures with desirable retention times for a diverse range of applications, including diagnostic imaging and optimal payload release with decreased nanotoxicity.

RESULTS AND DISCUSSION

Formulation of Tf-QD Conjugates. Tf-QDs (emission 525 nm, QD525), including holo- (iron saturated with carbonate as the synergistic anion), apo- (iron desaturated with carbonate as the synergistic anion), and oxa-Tf-QD (iron saturated with oxalate as the synergistic anion), were examined for their ability to modulate the intracellular retention of NPs. Bovine serum albumin−QDs (BSA-QDs) were also prepared as a control group. The protein−QD bioconjugates were prepared through ethyl(dimethylaminopropyl) carbodiimide (EDC)-mediated coupling between carboxyl-modified QDs and the primary amino groups of Tf. The conjugation of the QDs and proteins was examined using gel electrophoresis (see Figure S1a); the protein-tagged QDs (BSA: 67 kDa; Tf: 80 kDa) moved slower than the bare QDs. Figure S1b displays the spectrophotometric profiles of different protein−QD conjugates. The absorbance intensity varied depending on the nature of the modifying protein. The protein−QD bioconjugates and free QDs provided similar emission spectra. These results confirmed the conjugation of the QDs to the selected proteins. We used dynamic light scattering (DLS), a zeta potential analyzer, and inductively coupled plasma−mass spectrometry (ICP-MS) to measure the hydrodynamic sizes, particle surface charges, and protein occupancy[28] of the proteins conjugated to the QDs, respectively, for the various protein−QD bioconjugates (Table S1). The sizes of the three types of Tf-QDs (apo, holo, oxa) ranged from 22 to 25 nm (Figure S2); their zeta potentials ranged from −40 to −42 mV; the occupancy of the conjugated proteins to the QDs ranged approximately from 9 to 11. These data reveal that the three

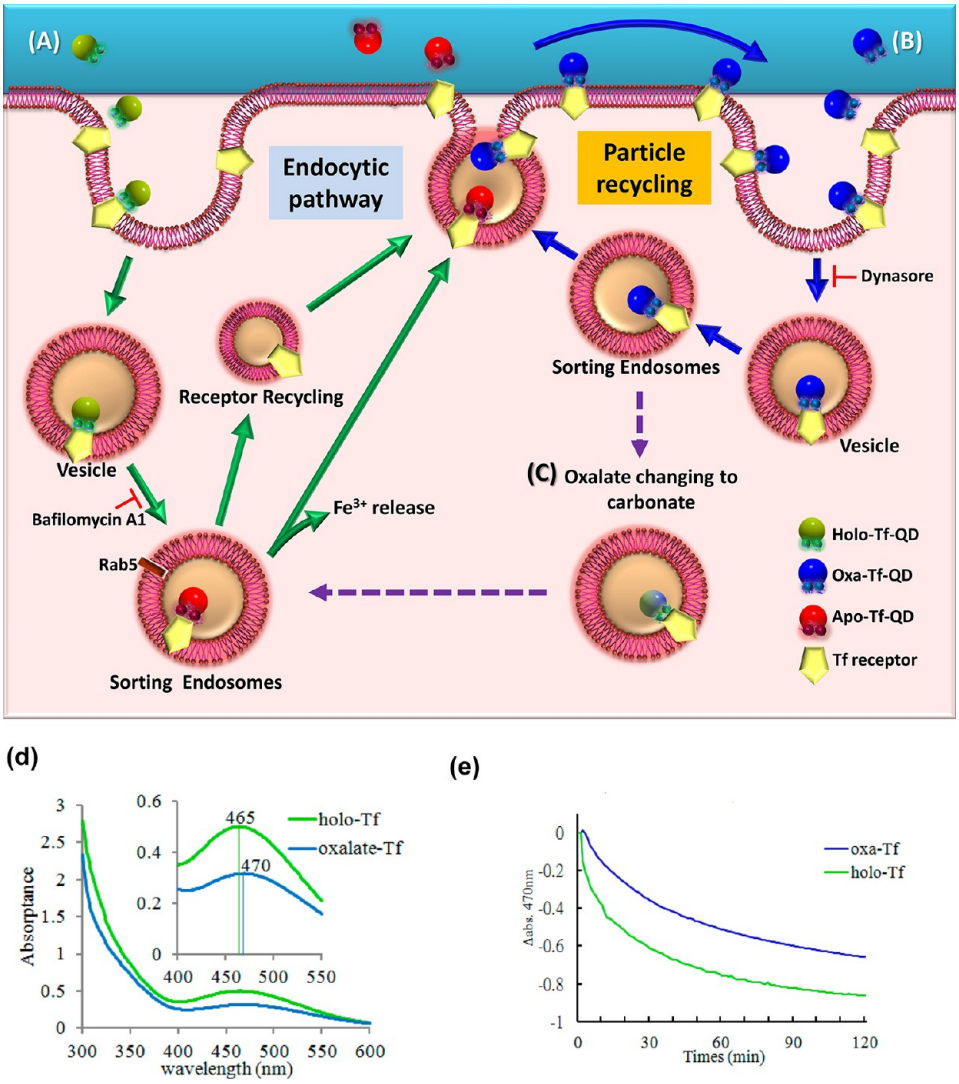

Figure 1. Schematic representation of intracellular retention of Tf-QD conjugates. (a) Holo-Tf-QD conjugates bind to Tf receptors and are then internalized by cells. They release iron in the endosomes at pH 5−6, subsequently forming apo-Tf conjugates. The apo-Tf-QD conjugates dissociate from the Tf receptors and are removed from cells. Meanwhile, Tf receptors are recycled by returning to the cell surface and waiting for the next cycle. (b) Oxa-Tf-QDs/Tf receptor complexes recycle from the endosomes to the cell surface and undergo reuptake by cells. This recycling results from the replacement of carbonate with oxalate, which retards iron release in endosomes. Oxa-Tf-QD conjugates remain bound to the Tf receptors, undergoing cellular recycling until (c) the oxalate is replaced by carbonate, with subsequent release of iron, leading to their cellular removal. (d) Iron loading and (e) releasing profiles of holo- and oxa-Tf conjugates at endosomal pH 5.6.

types of Tf-QDs exhibited comparable physicochemical characteristics, except for the nature of the synergistic anions (carbonate *vs* oxalate).

Because the iron-release rate of oxalate-replaced Tf derivatives is approximately 87-fold slower than those of the carbonate analogues,[22] we wished to use our oxalate-replaced Tf derivatives as NP cellular targeting ligands to modulate the intracellular NP retention time. Figure 1a−c illustrates the concept of modulating the intracellular NP retention and the characteristics of the various protein−QD conjugates. The iron loading and releasing of holo- and oxa-Tf-QDs were examined.[22] We measured the iron loadings of the holo- and oxa-Tf-QDs at 465 and 470 nm, respectively (Figure 1d) and their iron releasing at 470 nm (Figure 1e). The iron-release profile of the oxa-Tf-QDs was significantly slower than that of the holo-Tf-QDs. As illustrated in Figure 1a, holo-Tf conjugates are internalized into cells after binding to Tf receptors. They release iron in the endosomes at pH 5−6, consequently forming apo-Tf conjugates, which dissociate from Tf receptors and become removed from the cells. Meanwhile, the Tf receptors are recycled to the cell surface, where they wait for the next cycle. On the other hand, oxa-Tf-QDs/Tf receptor complexes (Figure 1b) underwent recycling from the endosomes to the cell surface and then were subjected to reuptake by the cells. This enhanced recycling resulted from replacement of carbonate by oxalate, that is, because of the retarded release of iron in endosomes. The oxa-Tf-QD conjugates remained

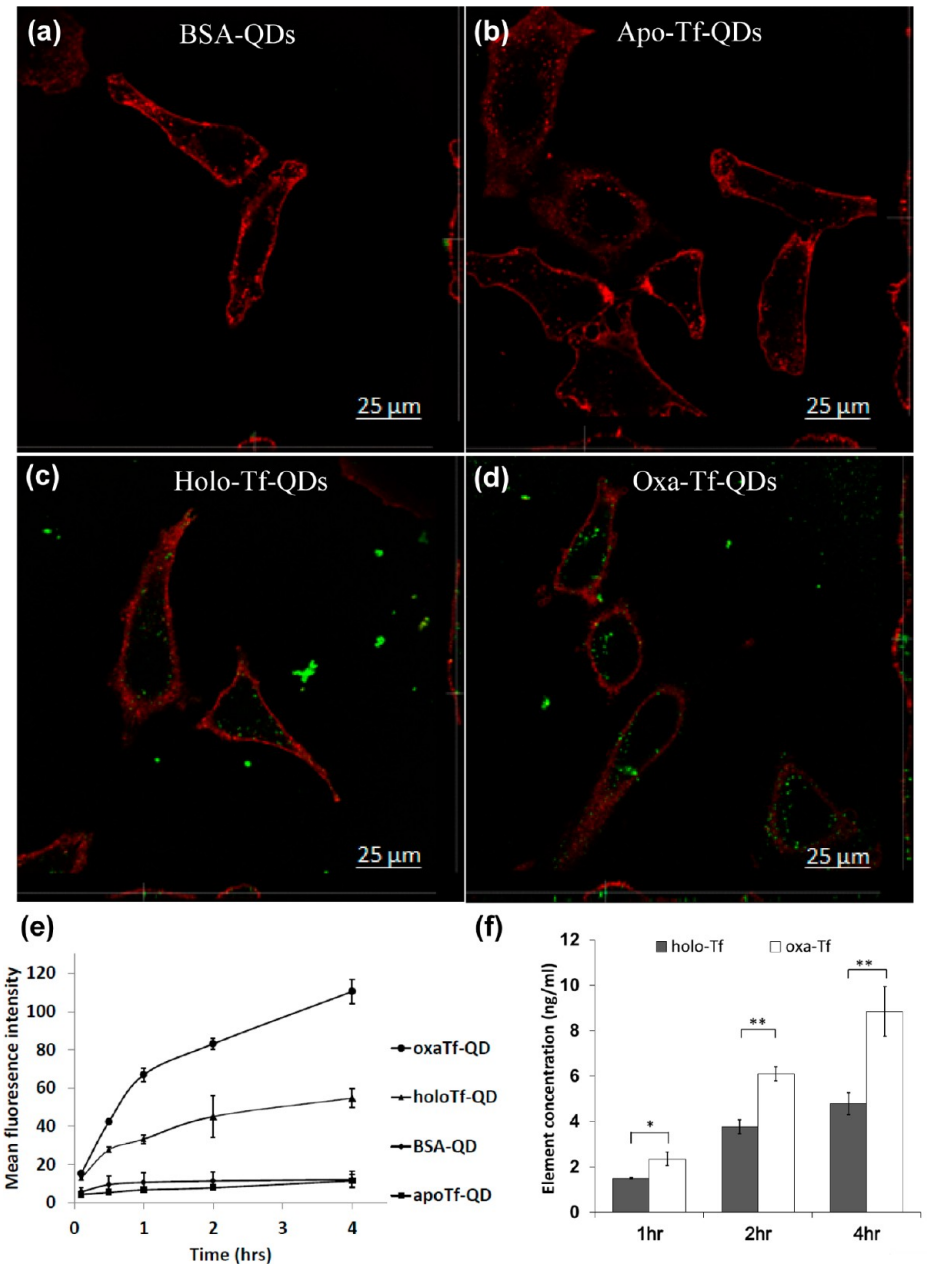

Figure 2. Internalization of Tf-QDs by HeLa cells. (a–d) Fluorescence confocal microscopy images of internalized protein–QD bioconjugates in HeLa cells. Notably, low or no fluorescence intensity appears for the (a) BSA-QDs and (b) apo-Tf-QDs; higher fluorescence intensity appears for the (c) holo-Tf-QDs and (d) oxa-Tf-QDs. (e) Time study of the cellular internalization of the protein–QD bioconjugates BSA-QD, apoTf-QD, holoTf-QD, and oxaTf-QD, determined using flow cytometry. (f) ICP-MS quantification of Cd in holo-Tf-QD and oxa-Tf-QD after various incubation periods (*$p < 0.05$, **$p < 0.01$).

bound to the Tf receptors to undergo cellular recycling until the oxalate was replaced by carbonate (Figure 1c) with subsequent iron release, leading to their cellular removal.

Intracellular NP Retention of Tf-QDs in HeLa cells. Figure 2 depicts the cellular accumulation of the different types of Tf-QDs in HeLa cells. After 2 h of incubation, the accumulation of the BSA-Tf-QDs was lower than those of the others (Figure 2a). The apo-Tf-QDs accumulated to a low level because of the absence of iron in the Tf moieties (Figure 2b). On the other hand, the accumulation of the holo- and oxa-Tf-QDs resulted in enhanced fluorescence in HeLa cells (Figure 2c, d). After 2 h of incubation, the oxa-Tf-QDs provided the highest level of cellular fluorescence. Analyses using flow cytometry (Figure 2e) and ICP-MS (Figure 2f) provided results similar to those from confocal microscopic analysis. The cellular mean fluorescence intensity (MFI) of the apo-Tf-QDs did not increase upon increasing the incubation period, whereas the MFI ($p < 0.05$) increase was significant for both the holo- and oxa-Tf-QDs, with the latter exhibiting a 1.8-fold-higher MFI than that of the former 2 h after treatment (82.5% *vs* 45% for oxa- and holo-Tf-QD, respectively). ICP-MS analysis confirmed that

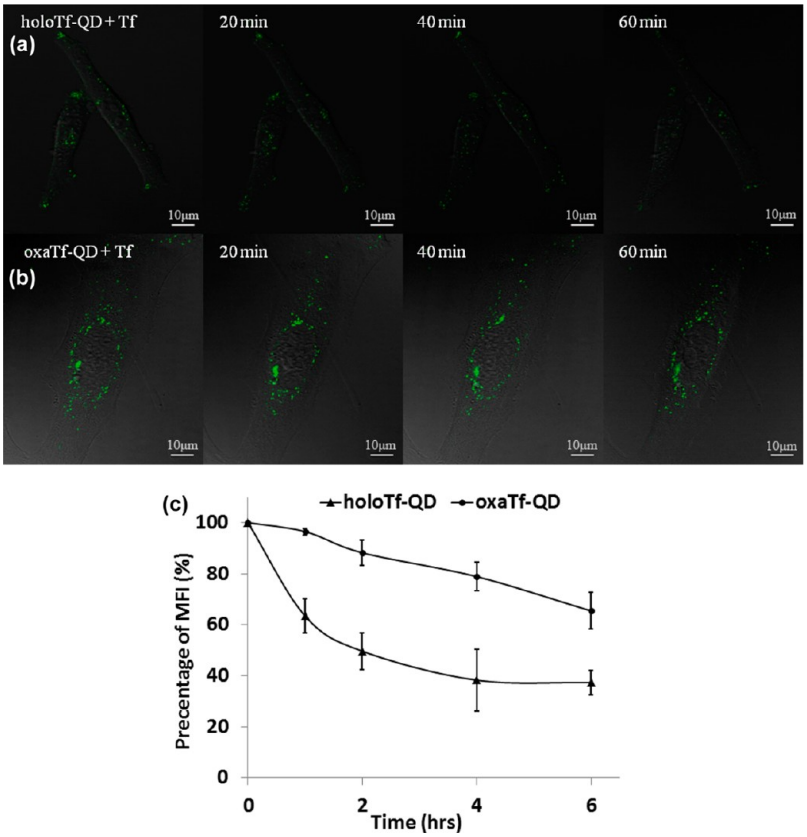

Figure 3. Release profiles of holo-Tf-QD and oxa-Tf-QD in HeLa cells. HeLa cells were preincubated with (a) holo- and (b) oxa-Tf-QDs (20 nM) for 2 h. After washing with PBS, these cells were cultured with unbound free Tf (2.5 mg/mL; serum Tf concentration). Confocal microscopy images were recorded at designated time points (20, 40, 60 min) after administration of free Tf. Free unconjugated Tf competed with the Tf-QDs for the limited TfRs. (c) Flow cytometric analysis at designated time points (1, 2, 4, and 6 h) after treatment with free Tf. Each measurement was conducted in triplicate.

the intracellular accumulation of the oxa-Tf-QDs was greater than that of the holo-Tf-QDs (6.2 *vs* 3.8 ng/mL for oxa- and holo-Tf-QD, respectively) (Figure 2f). These results suggested that the nature of the Tf synergistic anions (carbonate or oxalate) markedly affected the level of cellular accumulation of the Tf-QDs. The increased accumulation of the oxa-Tf-QDs presumably resulted from extended NP cellular retention intervals, possibly caused by oxa-Tf-QD-induced delay of cellular removal.

To further examine this hypothesis, we analyzed the cellular removal of the various Tf-QDs (Figure 3). After preincubating the HeLa cells with the holo- and oxa-Tf-QDs (20 nM) for 2 h, we washed the cells with PBS and then cultured them with unbound free Tf (2.5 mg/mL; serum Tf concentration). Free unconjugated Tf would compete with the Tf-QDs for the limited number of TfRs, thereby decreasing the rebinding of the Tf-QDs to the TfRs and triggering the removal of the intracellular Tf-QDs, as observed by the decline in the cellular fluorescent intensity. Confocal microscopic analysis (at 20, 40, and 60 min after administration of free Tf) revealed (Figure 3a, b) that the fluorescence intensity of both the holo- and oxa-Tf-QDs decreased, indicating that these two types of Tf-QDs could compete with free Tf for the TfRs. Increasingly more TfRs were gradually occupied by the free Tf, leading to limited cycling of the Tf-QDs. Similarly, flow cytometric analysis (at 1, 2, 4, and 6 h after treatment) revealed that the MFIs of the holo- and oxa-Tf-QDs both decreased, indicating the removal of these NPs from the cells. Notably, the MFI of the oxa-Tf-QDs was approximately 1.6 times higher than that of the holo-Tf-QDs (88 *vs* 50, respectively, at 2 h; Figure 3c), implying that the oxa-Tf-QDs were detained by the HeLa cells, leading to delayed cellular removal. On the basis of these results (Figures 2 and 3), the nature of the synergistic anion appears to significantly influence the cellular accumulation of the NPs. The cellular behavior of the oxa-Tf-QDs revealed that their increased accumulation resulted from their delayed cellular removal, which led to extended intracellular retention periods.

Mechanism of Oxa-Tf-QD-Induced Change in Intracellular Retention Interval in HeLa Cells. The variation in the oxa-Tf-QD-induced intracellular retention interval might possibly have resulted from reentry of the oxa-Tf-QD/TfR complexes into cells and retardation of endosomal Tf iron release.[22] We investigated the mechanisms behind the variations in intracellular retention through the arrest of endocytosis and the inhibition of endosomal acidification. We used dynasore, a cell-permeable

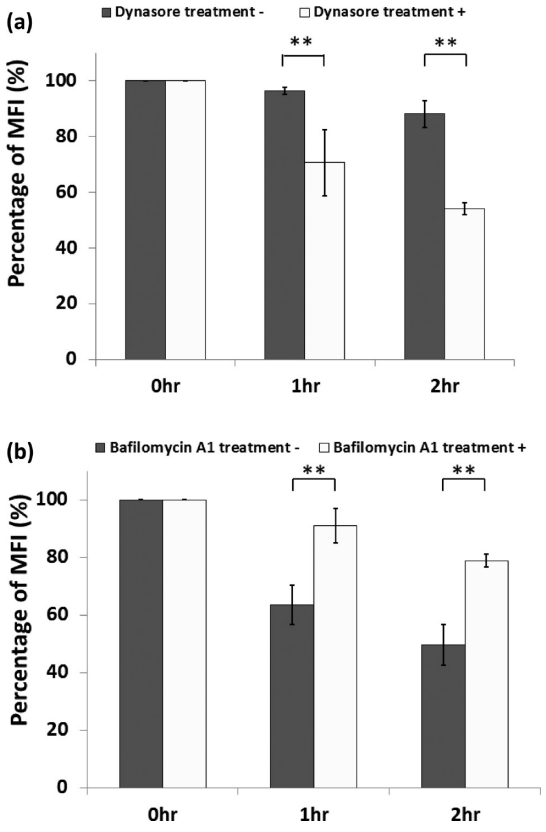

Figure 4. Mechanisms of the cellular recycling of oxaTf-QDs in HeLa cells. The cellular recycling mechanisms were investigated in terms of (a) the arrest of endocytosis (treatment with dynasore) and (b) the inhibition of endosomal acidification (treatment with bafilomycin A1). HeLa cells were precultured with (a) oxa-Tf-QDs or (b) holo-Tf-QDs for 2 h and then subjected to a series of washes before being co-incubated with free Tf (2.5 mg/mL) and dynasore (80 μM) or bafilomycin A1 (250 nM) for designated periods of time. Flow cytometric analysis was performed after treatment for 0, 1, and 2 h. Each measurement was conducted in triplicate (*$p < 0.05$, **$p < 0.01$).

inhibitor of dynamin, to suppress the receptor recycling pathway by arresting dynamin-dependent endocytosis and the scission of newly generated vesicles from membranes of cellular compartments. After preculturing the HeLa cells with oxa-Tf-QDs for 2 h, we subjected the cells to a series of washes and then co-incubated them with free Tf (2.5 mg/mL) and dynasore (80 μM). Figure 4a presents the results from flow cytometric analysis of the HeLa cells after treatment with dynasore for 2 h. The MFIs of the dynasore-treated groups decreased more significantly ($p < 0.05$) than those that had not been treated (70 *vs* 98% at 1 h; 58 *vs* 90% at 2 h, respectively), indicating the inhibition of reinternalization. These observations suggested that oxa-Tf-QD-induced variation in the intracellular retention interval resulted partly from cellular recycling of the Tf/TfR complexes.

After confirming the cellular recycling of Tf-QD/TfR complexes, we were interested in whether endosomal iron release was also a key factor affecting the variation in the retention period, because recycling of the oxa-Tf-QDs was partly caused by the stabilized Tf/TfR complexes and was dependent on iron binding. We used bafilomycin A1 (250 nM), an inhibitor of vacuolar H^+-ATPases (V-ATPase) on endosomes, to inhibit endosomal acidification, leading to the disrupted Tf iron release. After preculturing the HeLa cells with holo-Tf-QDs for 2 h, we subjected them to a series of washes and then co-incubated them with free Tf (2.5 mg/mL) and bafilomycin A1 (250 nM) for 2 h. As displayed in Figure 4b, the MFIs of the bafilomycin A1-treated groups were significantly higher than those of the nontreated groups (91% *vs* 64% at 1 h; 79% *vs* 50% at 2 h, respectively). These data suggested that inhibition of endosomal acidification could retard iron release from the holo-Tf-QDs, leading to elevated levels of accumulated holo-Tf-QDs. On the basis of these results, the inhibition of iron release from Tf, through either the endosomal acidification inhibitory system (holo-Tf-QDs) or the synergistic anion replacement system (oxa-Tf-QDs), was a vital element in the variations of the NP intracellular retention periods.

Effect of Tf Synergistic Anion on the Direction of Intracellular Tf-QD Trafficking Route in HeLa Cells. It has been suggested that the size of a Tf-conjugated NP (TCNP) plays a critical role in directing its intracellular trafficking routes.[12] When NPs are larger than 50 nm,[13] they become incorporated into late endosomes,[29] subsequently fusing with and accumulating in lysosomes. These large TCNPs may reside intracellularly for long periods of time before they are excytosed. In contrast, TCNPs that are less than approximately 30 nm[14] enter the early endosomes and recycle to the cell surface. These observations suggested that the particle size is one of the decisive factors affecting the NP intracellular trafficking route. Therefore, we examined whether substitution of the Tf synergistic anion (oxa-Tf-QDs *vs* holo-Tf-QDs) resulted in redirection of the Tf-QD trafficking route through tracking of the intracellular localization of these endocytosed Tf-QDs. Herein, we used Rab5-RFP, expressed in early endosomes, and Red DND-99, a lysotracker for the identification of acidic organelles such as late endosomes and lysosomes, to track the intracellular localization of the Tf-QDs. Confocal microscopy revealed that the intracellular holo- and oxa-Tf-QDs were co-localized with Rab5-RFP (Figure 5a, b), but neither were co-localized with lysosomes (Figure 5c, d). These results suggested that the intracellular localization of oxa-Tf-QD, similar to that of holo-Tf-QD, involved existence in early endosomes, but not much in acidic organelles or lysosomes.[12,14,30]

Moreover, TEM analysis revealed similar localization of oxa-Tf-QD and holo-Tf-QD, in that they were both wrapped up in a 200 nm endosome-like vacuole (Figure 5e, f). Notably, the accumulation of the oxa-Tf-QDs was greater than that of the holo-Tf-QDs (Figure 2f). Because the holo- and oxa-Tf-QDs underwent

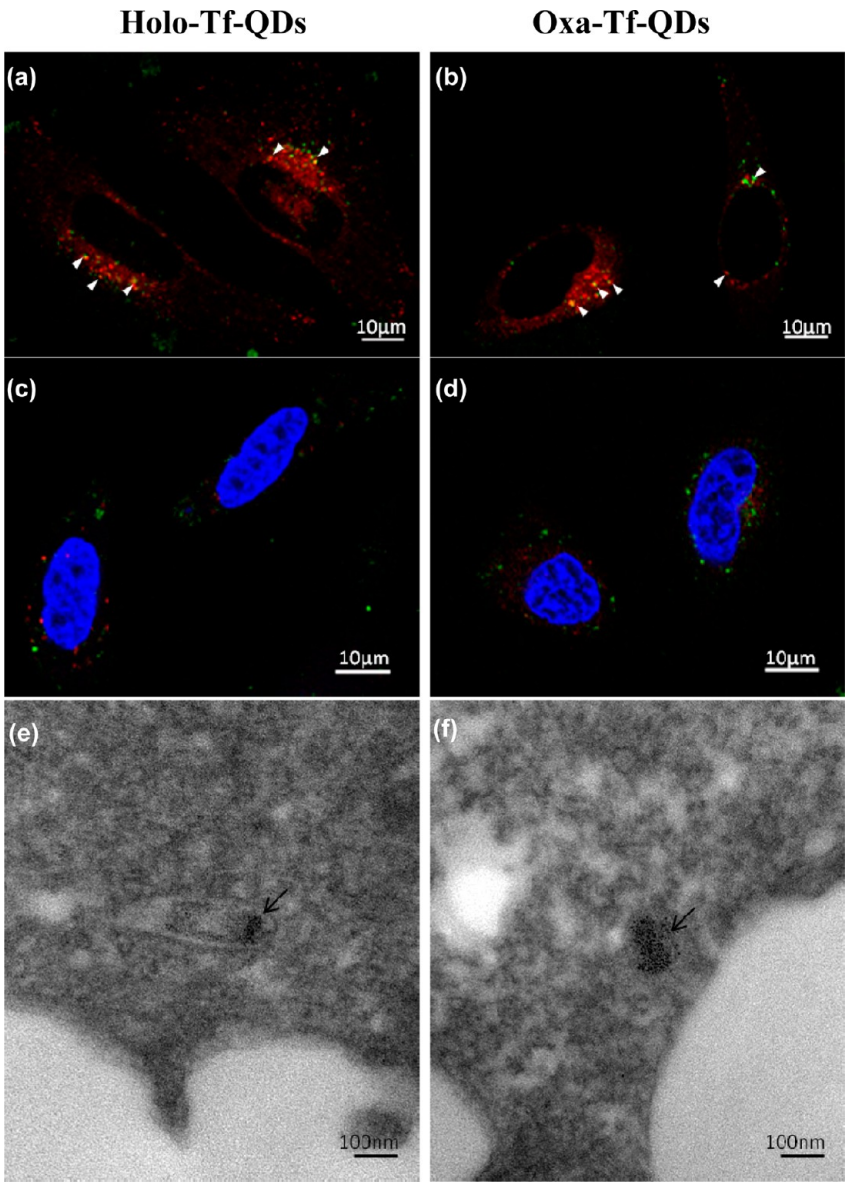

Figure 5. Co-localization of holo-Tf-QDs and oxa-Tf-QDs in HeLa cells. (a, b) Rab5-RFP was used to trace the localization of (a) holo-Tf-QDs and (b) oxa-Tf-QDs. Rab5-RFP was expressed in early endosomes. Arrows indicate the co-localization of Tf-QDs and early endosomes. (c, d) Red DND-99, a lysotracker, was used to identify late endosomes and lysosomes in cells treated with (c) holo-Tf-QDs and (d) oxa-Tf-QDs. (e, f) TEM analysis of (e) holo-Tf-QDs and (f) oxa-Tf-QDs. Arrows indicate the existence of Tf-QDs in endosome-like vacuoles.

comparable intracellular localization, these observations suggested that substitution of the Tf synergistic anions did not redirect the Tf-QD trafficking route, but instead increased the degree of particle accumulation.

Programmable Tf-QD Intracellular Retention Periods. The intracellular Tf-QD retention period could be programmed by adjusting the ratio of oxa- and holo-Tfs on the QD surfaces to manipulate the NP intracellular retention interval through control of the cellular recycling levels of the Tf/TfR complexes (Figure 6). At a ratio of 1:1 (holo-Tf:oxa-Tf), the MFI of the mixed-Tf-QDs (78%) was between those of the pure oxa- (86%) and pure holo-Tf-QDs (52%), indicating that the recycling of the Tf-QDs could be "ratio-dependently" programmed. Accordingly, manipulation of the oxa-/holo-Tf ratio on QD surfaces may provide a means of programming intracellular NP retention time, potentially improving imaging or the efficacy of therapeutic nanodelivery.

***In Vivo* Retention Profile of Tf-QDs in A549 Xenograft Tumor Models.** We used the oxa-Tf-QDs in imaging studies to investigate whether the synergistic anion effect was applied *in vivo*. After injecting various Tf-QDs (BSA-, apo-, holo-, and oxa-Tf-QDs) intratumorally, we used a spectrophotometric system to measure the emitted fluorescence at different time intervals (1, 30, 60, and 120 min; 24 h). The fluorescence intensities (Figure 7) revealed that the oxa-Tf-QDs exhibited the highest fluorescence intensity among the tested group.

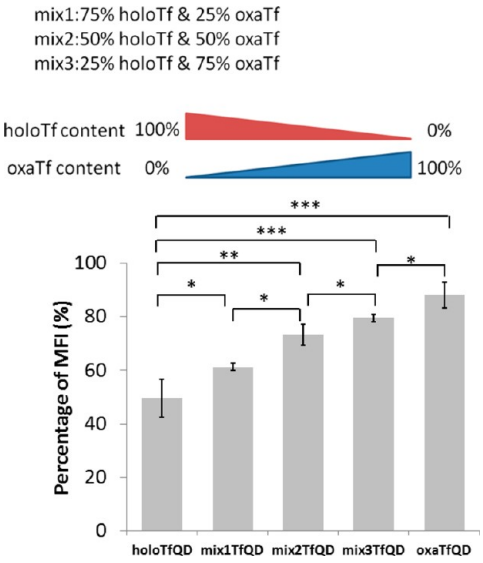

Figure 6. Programmable intracellular retention of Tf-QDs. Tf-QDs presenting holo- and oxa-Tf at ratios of 75:25, 50:50, and 25:75 were used to program the cellular retention of NPs. HeLa cells were incubated in serum-free MEM with Tf-QD (20 nM) at 37 °C for 2 h. Cells were then washed twice with PBS and stripping solution, trypsinized, and collected for FACS analysis (*$p < 0.05$, **$p < 0.01$, ***$p < 0.001$).

The fluorescence intensity of the negative control groups (BSA- and apo-Tf-QDs) was not higher than those of the holo- and oxa-Tf-QDs. The half-maximum fluorescence intensity of the holo-Tf-QDs was approximately 30 min after injection, whereas that of the oxa-Tf-QDs was 4-fold longer at approximately 2.2 h. Notably, the endogenous concentration of serum Tf was approximately 2.5 mg/mL. These unbound Tf units would compete with the injected Tf-QDs for available TfRs, potentially decreasing the cellular retention of the Tf-QDs *in vivo*. Our results revealed that the cellular retention of the oxa-Tf-QDs was longer than that of their holo-form counterparts, both *in vivo* and *in vitro*. Thus, the substitution of oxalate for carbonate in Tf significantly extended the cellular retention time. Therefore, the NP intracellular retention period can be manipulated *in vitro* and *in vivo* through substitution of Tf synergistic anions to interfere with the iron release from Tf. Retarded iron release would stabilize Tf/TfR complexes and, thereby, promote cellular recycling of these complexes.

Our results have several important implications for the use of nanodelivery systems in therapeutic and imaging applications. Substitution of the synergistic anions of Tf allows the intracellular NP retention periods

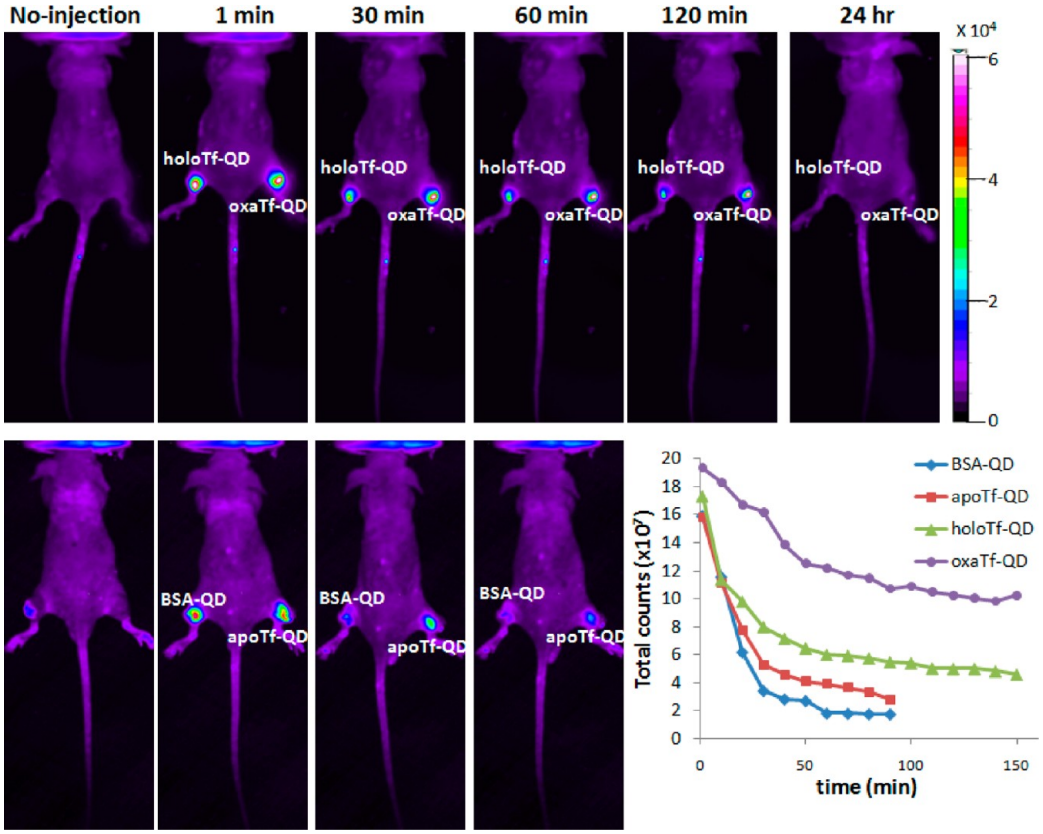

Figure 7. Tumor retention profiles of various protein−QD bioconjugates in A549 xenograft tumor. Various Tf-QDs, including BSA-, apo-, holo-, and oxa-Tf-QDs, were injected intratumorally. The emitted fluorescence was observed after various time intervals (1, 30, 60, and 120 min; 24 h) and collected using a spectrophotometric system (Xenogen/Caliper IVIS-200 *in vivo* imaging system). Mice were anesthetized with 2.5% isoflurane (ip). Using a heating pad, the animal body temperatures were maintained at 37 °C. The animals (nude mice, 20 g, 6−8 weeks old) were fasted for 12 h prior to imaging to reduce rodent chow autofluorescence within the GI tract. Images were recorded for 1 min after each 10 min interval after the injection of the QD solution (0.1 mL, 100 nM in PBS). The fluorescence signals were then quantified by using Living Image software.

of Tf-conjugated NPs (25 nm) to be manipulated. This approach has the potential to enhance the function and efficacy of designed nanomaterials and to compensate for the low *in vivo* accumulation of introduced NPs, for example, in tumor tissues, where it is generally approximately 2−3% of the injected dosage in both targeted and untargeted delivery.[4] Nanoparticles modified with oxalate-replaced Tf exhibit extended intracellular retention periods because they decrease the degree of NP cellular removal, caused by stabilized Tf/TfR complexes and their subsequent cellular recycling. In this study, we achieved Tf/TfR complex stabilization through oxalate-induced disruption of endosomal Tf iron release, which resulted in enhanced interaction of Tf/TfR. In addition, through the immobilization of oxalate- and carbonate-Tfs at various ratios on the surfaces of the NPs, we could tailor the intracellular retention time to a desirable level for specific applications. However, it is possible that the modification of synergistic anions may make limited changes in the total retention time for larger particles (*e.g.*, ∼50 nm) due to their incorporation into late endosomes/lysosomes.

This simple approach is quite easy to perform. Unlike the conventional approach toward intracellular retention through manipulation of particle sizes, often troublesome because of the need to prepare uniformly special sized nanostructures, our present method toward tunable retention periods depends solely on substitution of the synergistic anions of the conjugated ligands (Tf). In a recent investigation of the effect of the ligand content of Tf on AuNPs,[4] a high Tf content tended to result in the AuNPs being accumulated within cancer cells. Similarly, the oxa-Tf-QDs in our present study also accumulated to higher degrees relative to counterparts in HeLa cells both *in vitro* and *in vivo*. These results further demonstrate the effectiveness and significance of our developed approach, which grants us a convenient means of improving the performance of nanodelivery systems.

Moreover, we anticipate that a series of anions (*e.g.*, malonate, glycolate) with various iron-release abilities[26,27] could be selected as substituting agents for carbonate. Different synergistic anions would presumably result in distinct retention times because they would vary the strength of ligand−receptor binding; in the near future, we will report our findings on the effect of substitution with other synergistic anions on intracellular retention. We stress that the oxalate-substituted Tf studied herein was merely a model to prove the concept of regulating the intracellular NP retention time. It is likely that other diverse features of certain ligand−receptor interactions could be used to manage the NP retention periods. Furthermore, synergistic anion-replaced Tf derivatives (*e.g.*, oxa-Tf) could presumably be incorporated with other targeting ligands on NPs for multiligand binding. These NPs might, therefore, undergo target identification first, followed by triggering of cell internalization for designed intracellular periods. With this fascinating tool in hand, the intracellular retention times of nanodelivery systems could be programmed; meanwhile, the imaging and therapeutic efficacy might also be enhanced.

CONCLUSION

In summary, replacing the synergistic anions of Tf on NPs can provide a nanodelivery system with the following features: (1) a programmable intracellular retention time; (2) an intracellular trafficking pathway similar to holo-Tf-QDs; and (3) a simple, easy, and cost-effective protocol. We focused on the manipulation of intracellular retention time of nanoparticles with the characteristic of rapid tumor permeation (∼20 nm) to improve their tumor accumulation and to avoid the nanotoxicity observed in larger sized NPs (∼50 nm). A desired level of NP retention can be achieved through adjustment of the nature of the synergistic anion of Tf or the ratio of Tf with different synergistic anions. This design can improve not only the targeting efficiency of nanomaterials but also potentially the safety and therapeutic efficacy of nanoformulations. Future works will attempt to study whether the synergistic anion substitution effect could be applied on other sized nanoparticles to increase their cellular accumulation through the manipulation of intracellular retention time.

MATERIALS AND METHODS

Preparation of Oxalate-Transferrin. Oxa-Tf was prepared, using a modification of the procedure reported by Everse *et al.*,[22] through the addition of two equivalents of Fe(III)-nitrilotriacetate (NTA), with the iron and NTA premixed at a ratio of 1:2, to apo-Tf in 20 mM potassium oxalate. The mixture was incubated at room temperature for 1 h, followed by exhaustive exchange into 10 mM KCl containing 10 mM potassium oxalate using Centricon 10 microconcentrators (Milipore, Billerica, MA, USA). Free oxalate was removed by passing through a PD-10 desalting column (GE Healthcare, Piscataway, NJ, USA), eluting with 10 mM borate buffer (pH 8.0), to avoid interference in the subsequent EDC/*N*-hydroxysuccinimide (NHS) reaction.

Bioconjugation of Quantum Dots. Tf-modified quantum dots were prepared through conjugation of Tf (holo- and oxalate-replaced forms) with carboxyl quantum dots (Qdot ITKTM carboxyl, Invitrogen, Grand Island, NY, USA) *via* EDC/NHS coupling reactions. The QDs were mixed with EDC and NHS in 10 mM borate buffer (pH 8.0) to activate the QD carboxyl groups at room temperature for 1 h. Protein conjugation was performed by adding proteins into the QD conjugation reaction solution at room temperature. After incubation for 1 h, the protein−QD conjugation reaction mixture was centrifuged at 3000*g*, using a 100 kD centrifugal filter (Milipore, Billerica, MA, USA) to remove free protein and excessive reagents. QD analyses were performed on the basis of quantification of ^{111}Cd and ^{78}Se concentrations using ICP-MS (Elan6100; PerkinElmer, Shelton, CT, USA).[31] The protein contents of the protein−QDs were measured using protein assay kits (Bio-Rad, Hercules, CA, USA).

PA-AGE Gel Preparation and Electrophoresis. Hybrid gels composed of 2% polyacrylamide (PA) and 0.5% agarose (AGE) were

prepared for QD-based PA-AGE electrophoresis analysis.[32] Equal volumes of 1% AGE and 4% PA were mixed, and then ammonium persulfate [to a final concentration of 0.05% (w/v)] and TEMED (1:5000, v/v) were added. Electrophoresis was performed at 90−150 V for 1−2 h. The running buffer was 0.5× TAE buffer containing 0.1% SDS.

Particle Characterization: Transmission Electron Microscopy Imaging of Protein−QDs. Protein−QD complexes were imaged using a Hitachi H-7650 transmission electron microscope operated at 80 kV. Diluted QDs were dissolved in ddH_2O and placed onto a Formvar-coated Cu grid. For negative staining, the grids were treated with 1% uranyl acetate (5 μL) for 40 s and then dried in a vacuum hood.

Particle Size and Zeta Potential Measurements. The hydrodynamic diameters and zeta potentials of the particles were measured using dynamic light scattering on a Malvern Zetasizer Nano system (Malvern, Worcestershire, UK) equipped with a 633 nm laser. The relationship between the sizes of particles and their Brownian motion is described by the Stokes−Einstein equation.[33] The zeta potentials of particles influence their electrophoresis and mobility, as determined by the Henry equation and the Smoluchowski approximation.[34] The concentration of the QDs was 2−3 μM. The QDs were dispersed in ddH_2O at a concentration of 0.3 μM, and the zeta potential was measured. Hydrodynamic sizes and zeta potentials are reported herein as means of triplicate measurements ± SD.

Kinetics of Iron Release from Holo-Tf and Oxalate-Tf. Iron-release reactions were performed according to Woodworth *et al.*[35] in a quartz cuvette and monitored using UV−Vis spectroscopy. Iron-loaded Tf was filtered (0.2 μm Acrodisc filters; Gelman Sciences, Ann Arbor, MI, USA) and added into a sample cuvette containing 2-(*N*-morpholino)ethanesulfonic acid (MES)−EDTA buffer (pH 5.6) to a final protein concentration of 40−45 μM. The time of mixing in the MES−EDTA buffer (pH 5.6) was considered as the zero time. All samples were determined against a reference MES−EDTA buffer. The matched pairs of samples and references were equilibrated at 25 °C for 10−15 min prior to measurement. For measurement of the iron released from Tf, the absorbance decrease at a wavelength of 470 nm was monitored and recorded for 1 h. The measurements were conducted at least in triplicate.

Tf-QD Cellular Uptake and Removal. HeLa cells (2×10^5/well) were seeded and incubated in six-well culture plates for 24 h. For Tf-QD cellular uptake experiments, HeLa cells were incubated in serum-free MEM with the Tf-QDs (20 nM) at 37 °C for designated periods. At each time point (0.5, 1, 2, and 4 h), HeLa cells were washed twice with PBS and stripping solution (25 mM citric acid, 24.5 mM sodium citrate, 280 mM sucrose, pH 4.6) to remove nonspecifically bound Tf-QDs, trypsinized, and then collected in 15 mL centrifuge tubes for analysis through fluorescence-activated cell sorting (FACS). For Tf-QD cellular removal experiments, HeLa cells were incubated in serum-free MEM with the Tf-QDs (20 nM) at 37 °C for 2 h; the cells were then washed twice with PBS before being incubated in MEM with 1% FBS and free Tf (2.5 mg/mL) at 37 °C for designated periods. At each time point (1, 2, 4, and 6 h), cells were washed with PBS and stripping solution, trypsinized, and collected in 15 mL centrifuge tubes for FACS analysis. For the QD cellular removal inhibition experiments, HeLa cells were first incubated in MEM with 1% FBS and Tf-QDs (20 nM) for 2 h. After washing twice with PBS and stripping solution, the cells were incubated in MEM with 1% FBS, free Tf (2.5 mg/mL), and dynasore (80 μM) for different periods of time (1 and 2 h). For the endosome acidification inhibition experiments, HeLa cells were first incubated in MEM with 1% FBS, bafilomycin A1 (250 nM),[36] and the Tf-QDs (20 nM) for 2 h. After washing twice with PBS and stripping solution, the cells were incubated in MEM with 1% FBS, free Tf (2.5 mg/mL), and Bafilomycin A1 (250 nM) for different periods of time (1 and 2 h). Finally, the cells were washed and collected for analyses through FACS and confocal microscopy.

Quantification of Tf-QDs in Cells through FACS Analysis. HeLa cells (2×10^5/well) were cultured in serum-free MEM with Tf-QDs (20 nM) at 37 °C for designated periods (1, 2, 4, and 6 h). After washing twice with PBS and stripping solution, the cells were centrifuged (100*g*) and subjected to flow cytometric analysis (FACS Calibur, BD Biosciences, San Jose, CA, USA).

Confocal Microscopy Imaging. HeLa cells were plated onto 35 mm Petri dishes with a thin bottom for high-end microscopy (Ibidi, Madison, WI, USA) and incubated in low-serum MEM (1% FBS) containing Tf-QDs (20 nM) at 37 °C, 5% CO_2 for 2 h. At each time point, the cells were washed with fresh culture medium and examined using a Leica TCS SPE confocal laser scanning microscope (Leica, Wetzlar, Germany) equipped with CO_2 and temperature control. QDs and QD conjugates were excited with an Ar laser (488 nm) with emission channels of 500−540 nm for QDs. WGA594, Lysotracker Red DND99, and Rab5-RFP were excited with the 535 nm laser with emission channels of 570−625 nm. Hoechst33342 was excited with the 405 nm laser with emission channels of 460−480 nm.[29] Identification of the QDs' intracellular localization (cell membranes, nuclei, lysosomes) was performed by incubating fluorescent dyes—WGA594 (5 μg/mL), Hoechst33342 (1 μg/mL), and Lysotracker Red DND-99 (0.5 μM) (Invitrogen, Carlsbad, CA, USA), respectively—with live cells for 15−30 min and then imaging them using confocal microscopy. For the labeling of early endosomes, HeLa cells were transfected with Rab5-red fluorescent protein (Rab5-RFP) plasmid through electroporation, and then they were seeded and incubated for 48 h. Rab5, a small GTPase located at early endosomes, functions as a regulator for the fusion between endocytic vesicles and early endosomes.

Animals and Tumor Formation. Athymic nude mice (nu/nu; male, 6 weeks old or older, and weighing 20−24 g) were used for human lung carcinoma cell (A549) tumor xenografts. A549 cells were cultured in F12K supplemented with 10% FBS, penicillin (100 units/mL), and streptomycin (100 units/mL). Trypsinized A549 cells, during the exponential phase of growth, were resuspended in PBS and Matrigel (BD Biosciences, San Jose, CA, USA) and injected (subcutaneous) into nude mice at 2×10^6 cells per mouse. Tumors were allowed to grow to 50−100 mm^3 in volume prior to introduction of the QDs and imaging.

***In Vivo* Fluorescence Imaging.** *In vivo* fluorescence imaging was performed using a commercial Xenogen/Caliper IVIS-200 *in vivo* Imaging System (Alameda, CA, USA). Light from a 100 W Hamamatsu Xe lamp was passed through fluorophore-dependent bandpass interference filters (545AF75, Omega Optical) to induce QD525 fluorescence. The imaging sensor was a charge-coupled device camera (DW436, Andor Technology), thermoelectrically cooled to −90 °C. Bandpass interference filters (FF495 Ex 02-25, Smerok, USA) were placed over a 50 mm f/1.2 lens (Nikon, Tokyo, Japan) to pass fluorescent light but block excitation light.[37] Mice were anesthetized with 2.5% isoflurane (ip). Each animal's body temperature was maintained at 37 °C using a heating pad. The animals (nude mice, 20 g, 6−8 weeks old) were fasted for 12 h prior to imaging to reduce rodent chow autofluorescence within the GI tract. Images were recoded for 1 min after each 10 min interval after injection of the QD solution (0.1 mL, 100 nM in PBS); fluorescence signals were then quantified using Living Image software.[36,37]

Conflict of Interest: The authors declare no competing financial interest.

Acknowledgment. This work was supported by National Science Council of Taiwan (99-2113-M-260-002-MY2, 99-2627-M-260-001-, 100-2627-M-260-001-).

Supporting Information Available: The characterizations of protein−QD bioconjugates and the DLS, TEM of Tf-QD bioconjugates. This material is available free of charge via the Internet at http://pubs.acs.org.

REFERENCES AND NOTES

1. Byrne, J. D.; Betancourt, T.; Brannon-Peppas, L. Active Targeting Schemes for Nanoparticle Systems in Cancer Therapeutics. *Adv. Drug Delivery Rev.* **2008**, *60*, 1615–1626.
2. Danhier, F.; Feron, O.; Préat, V. To Exploit the Tumor Microenvironment: Passive and Active Tumor Targeting of Nanocarriers for Anti-Cancer Drug Delivery. *J. Controlled Release* **2010**, *148*, 135–146.

3. Bartlett, D. W.; Su, H.; Hildebrandt, I. J.; Weber, W. A.; Davis, M. E. Impact of Tumor-Specific Targeting on the Biodistribution and Efficacy of siRNA Nanoparticles Measured by Multimodality *in Vivo* Imaging. *Proc. Natl. Acad. Sci. U. S. A.* **2007**, *104*, 15549–15554.
4. Choi, C. H. J.; Alabi, C. A.; Webster, P.; Davis, M. E. Mechanism of Active Targeting in Solid Tumors with Transferrin-Containing Gold Nanoparticles. *Proc. Natl. Acad. Sci. U. S. A.* **2010**, *107*, 1235–1240.
5. Huang, X.; Peng, X.; Wang, Y.; Wang, Y.; Shin, D. M.; El-Sayed, M. A.; Nie, S. A Reexamination of Active and Passive Tumor Targeting by Using Rod-Shaped Gold Nanocrystals and Covalently Conjugated Peptide Ligands. *ACS Nano* **2010**, *4*, 5887–5896.
6. Nam, J.; Won, N.; Jin, H.; Chung, H.; Kim, S. pH-Induced Aggregation of Gold Nanoparticles for Photothermal Cancer Therapy. *J. Am. Chem. Soc.* **2009**, *131*, 13639–13645.
7. Cho, E. C.; Glaus, C.; Chen, J.; Welch, M. J.; Xia, Y. Inorganic Nanoparticle-Based Contrast Agents for Molecular Imaging. *Trends Mol. Med.* **2010**, *16*, 561–573.
8. Gabizon, A.; Horowitz, A. T.; Goren, D.; Tzemach, D.; Shmeeda, H.; Zalipsky, S. *In Vivo* Fate of Folate-Targeted Polyethylene-Glycol Liposomes in Tumor-Bearing Mice. *Clin. Cancer Res.* **2003**, *9*, 6551–6559.
9. Montet, X.; Funovics, M.; Montet-Abou, K.; Weissleder, R.; Josephson, L. Multivalent Effects of RGD Peptides Obtained by Nanoparticle Display. *J. Med. Chem.* **2006**, *49*, 6087–6093.
10. Phillips, M. A.; Gran, M. L.; Peppas, N. A. Targeted Nanodelivery of Drugs and Diagnostics. *Nano Today* **2010**, *5*, 143–159.
11. Alexis, F.; Pridgen, E.; Molnar, L. K.; Farokhzad, O. C. Factors Affecting the Clearance and Biodistribution of Polymeric Nanoparticles. *Mol. Pharmaceutics* **2008**, *5*, 505–515.
12. Chithrani, B. D.; Chan, W. C. W. Elucidating the Mechanism of Cellular Uptake and Removal of Protein-Coated Gold Nanoparticles of Different Sizes and Shapes. *Nano Lett.* **2007**, *7*, 1542–1550.
13. Jiang, W.; KimBetty, Y. S.; Rutka, J. T.; ChanWarren, C. W. Nanoparticle-Mediated Cellular Response is Size-Dependent. *Nat. Nanotechnol.* **2008**, *3*, 145–150.
14. Jin, H.; Heller, D. A.; Sharma, R.; Strano, M. S. Size-Dependent Cellular Uptake and Expulsion of Single-Walled Carbon Nanotubes: Single Particle Tracking and a Generic Uptake Model for Nanoparticles. *ACS Nano* **2009**, *3*, 149–158.
15. Perrault, S. D.; Walkey, C.; Jennings, T.; Fischer, H. C.; Chan, W. C. W. Mediating Tumor Targeting Efficiency of Nanoparticles Through Design. *Nano Lett.* **2009**, *9*, 1909–1915.
16. Slowing, I. I.; Vivero-Escoto, J. L.; Zhao, Y.; Kandel, K.; Peeraphatdit, C.; Trewyn, B. G.; Lin, V. S. Y. Exocytosis of Mesoporous Silica Nanoparticles from Mammalian Cells: From Asymmetric Cell-to-Cell Transfer to Protein Harvesting. *Small* **2011**, *7*, 1526–1532.
17. Wang, J.; Tian, S.; Petros, R. A.; Napier, M. E.; DeSimone, J. M. The Complex Role of Multivalency in Nanoparticles Targeting the Transferrin Receptor for Cancer Therapies. *J. Am. Chem. Soc.* **2010**, *132*, 11306–11313.
18. Bellocq, N. C.; Pun, S. H.; Jensen, G. S.; Davis, M. E. Transferrin-Containing, Cyclodextrin Polymer-Based Particles for Tumor-Targeted Gene Delivery. *Bioconjugate Chem.* **2003**, *14*, 1122–1132.
19. Daniels, T. R.; Delgado, T.; Helguera, G.; Penichet, M. L. The Transferrin Receptor Part II: Targeted Delivery of Therapeutic Agents into Cancer Cells. *Clin. Immunol.* **2006**, *121*, 159–176.
20. Davis, M. E.; Zuckerman, J. E.; Choi, C. H. J.; Seligson, D.; Tolcher, A.; Alabi, C. A.; Yen, Y.; Heidel, J. D.; Ribas, A. Evidence of RNAi in Humans from Systemically Administered siRNA *via* Targeted Nanoparticles. *Nature* **2010**, *464*, 1067–U140.
21. Giannetti, A. M.; Snow, P. M.; Zak, O.; Bjorkman, P. J. Mechanism for Multiple Ligand Recognition by the Human Transferrin Receptor. *PLoS. Biol.* **2003**, *1*, 341–350.
22. Halbrooks, P. J.; Mason, A. B.; Adams, T. E.; Briggs, S. K.; Everse, S. J. The Oxalate Effect on Release of Iron from Human Serum Transferrin Explained. *J. Mol. Biol.* **2004**, *339*, 217–26.
23. Lao, B. J.; Tsai, W.-L. P.; Mashayekhi, F.; Pham, E. A.; Mason, A. B.; Kamei, D. T. Inhibition of Transferrin Iron Release Increases *in Vitro* Drug Carrier Efficacy. *J. Controlled Release* **2007**, *117*, 403–412.
24. Prabaharan, M.; Grailer, J. J.; Pilla, S.; Steeber, D. A.; Gong, S. Amphiphilic Multi-Arm-Block Copolymer Conjugated with Doxorubicin *via* pH-Sensitive Hydrazone Bond for Tumor-Targeted Drug Delivery. *Biomaterials* **2009**, *30*, 5757–5766.
25. Bates, G. W.; Schlabach, M. R. The Nonspecific Binding of Fe^{3+} to Transferrin in the Absence of Synergistic Anions. *J. Biol. Chem.* **1975**, *250*, 2177–2181.
26. Schlabach, M. R.; Bates, G. W. The Synergistic Binding of Anions and Fe^{3+} by Transferrin. Implications for the Interlocking Sites Hypothesis. *J. Biol. Chem.* **1975**, *250*, 2182–2188.
27. Harris, W. R. Thermodynamics of Anion Binding to Human Serum Transferrin. *Biochemistry* **1985**, *24*, 7412–7418.
28. Huang, R. K.; Steinmetz, N. F.; Fu, C. Y.; Manchester, M.; Johnson, J. E. Transferrin-Mediated Targeting of Bacteriophage HK97 Nanoparticles into Tumor Cells. *Nanomedicine* **2011**, *6*, 55–68.
29. Zhang, L. W.; Monteiro-Riviere, N. A. Mechanisms of Quantum Dot Nanoparticle Cellular Uptake. *Toxicol. Sci.* **2009**, *110*, 138–55.
30. Iversen, T. G.; Skotland, T.; Sandvig, K. Endocytosis and Intracellular Transport of Nanoparticles: Present Knowledge and Need for Future Studies. *Nano Today* **2011**, *6*, 176–185.
31. Yang, R. S. H.; Chang, L. W.; Wu, J.-P.; Tsai, M.-H.; Wang, H.-J.; Kuo, Y.-C.; Yeh, T.-K.; Yang, C. S.; Lin, P. Persistent Tissue Kinetics and Redistribution of Nanoparticles, Quantum Dot 705, in Mice: ICP-MS Quantitative Assessment. *Environ. Health Perspect.* **2007**, 115.
32. Liu, H. Y.; Vu, T. Q. Identification of Quantum Dot Bioconjugates and Cellular Protein Co-localization by Hybrid Gel Blotting. *Nano Lett.* **2007**, *7*, 1044–1049.
33. Edward, J. T. Molecular Volumes and the Stokes-Einstein Equation. *J. Chem. Educ.* **1970**, *47*, 261.
34. Hunter, R. J. *Zeta Potential in Colloid Science: Principles and Applications*; Academic Press: London, 1981.
35. He, Q. Y.; Mason, A. B.; Woodworth, R. C. Iron Release from Recombinant N-Lobe and Single Point Asp(63) Mutants of Human Transferrin by EDTA. *Biochem. J.* **1997**, *328*, 439–445.
36. Presley, J. F.; Mayor, S.; McGraw, T. E.; Dunn, K. W.; Maxfield, F. R. Bafilomycin A1 Treatment Retards Transferrin Receptor Recycling More than Bulk Membrane Recycling. *J. Biol. Chem.* **1997**, *272*, 13929–13936.
37. Souris, J. S.; Lee, C.-H.; Cheng, S.-H.; Chen, C.-T.; Yang, C.-S.; Ho, J.-a. A.; Mou, C.-Y.; Lo, L.-W. Surface Charge-Mediated Rapid Hepatobiliary Excretion of Mesoporous Silica Nanoparticles. *Biomaterials* **2010**, *31*, 5564–5574.